

1 VeloViz: RNA-velocity informed embeddings for visualizing cellular trajectories

2 Lyla Atta^{1,2,3}, Arpan Sahoo^{1,4}, Jean Fan^{1,2,4,*}

3 ¹Center for Computational Biology, Whiting School of Engineering, Johns Hopkins University,

4 Baltimore, MD 21211, USA

5 ²Department of Biomedical Engineering, Johns Hopkins University, Baltimore, MD 21218, USA

6 ³Medical Scientist Training Program, Johns Hopkins University School of Medicine, Baltimore, MD

7 21205, USA

8 ⁴Department of Computer Science, Johns Hopkins University, Baltimore MD 21218, USA

9 *To whom correspondence should be addressed

10

11 Correspondence should be addressed to: Jean Fan (jeanfan@jhu.edu)

12

13 Key words: Bioinformatics, Computational biology, Gene expression, Single Cell, RNA velocity

14

15 **0 Abstract**

16 Single cell transcriptomic technologies enable genome-wide gene expression measurements in individual
17 cells but can only provide a static snapshot of cell states. RNA velocity analysis can infer cell state changes
18 from single cell transcriptomics data. To interpret these cell state changes as part of underlying cellular
19 trajectories, current approaches rely on visualization with principal components, t-distributed stochastic
20 neighbor embedding, and other 2D embeddings derived from the observed single cell transcriptional
21 states. However, these 2D embeddings can yield different representations of the underlying cellular
22 trajectories, hindering the interpretation of cell state changes. We developed VeloViz to create RNA-
23 velocity-informed 2D and 3D embeddings from single cell transcriptomics data. Using both real and
24 simulated data, we demonstrate that VeloViz embeddings are able to consistently capture underlying
25 cellular trajectories across diverse trajectory topologies, even when intermediate cell states may be
26 missing. By taking into consideration the predicted future transcriptional states from RNA velocity
27 analysis, VeloViz can help visualize a more reliable representation of underlying cellular trajectories.
28 VeloViz is available as an R package on GitHub (<https://github.com/JEFworks-Lab/veloviz>) with
29 additional tutorials at <https://JEF.works/veloviz/>.

30

31

32 **1 Introduction**

33

34 Current technologies for high-throughput single cell transcriptomics profiling provide a static snapshot of
35 the transcriptional states in individual cells. Still, the continuum of transcriptional states for cells along
36 dynamic processes such as organ development or tumorigenesis can be used to infer how cell states may
37 change over time (Tritschler *et al.*, 2019; Saelens *et al.*, 2019). Notably, RNA velocity analysis can be
38 applied to infer dynamics of gene expression and predict the future transcriptional state of a cell from
39 single cell RNA-sequencing and imaging data (La Manno *et al.*, 2018; Xia *et al.*, 2019).

40

41 To interpret such cell state changes from RNA velocity analysis, current approaches project the observed
42 current and predicted future transcriptional states onto 2-dimensional (2D) embeddings in order to
43 visualize the putative directed cellular trajectory (La Manno *et al.*, 2018; Zywitzka *et al.*, 2018; Bastidas-
44 Ponce *et al.*, 2019; Zhang *et al.*, 2019). Previously used 2D embeddings include those derived from
45 principal components (PC), t-distributed Stochastic Neighbor Embeddings (t-SNE), Uniform Manifold
46 Approximation and Projection (UMAP), and diffusion maps (Coifman *et al.*, 2005; Maaten and Hinton,
47 2008; McInnes *et al.*, 2018) established using the observed single cell transcriptional states. However,
48 these approaches can yield different representations of the underlying cellular trajectory. Furthermore, in
49 dynamic processes where intermediate cell states are not well represented due to their transient nature or
50 due to technical limitations in sample collection and processing, current 2D embeddings may be unable
51 to capture global relationships between cell subpopulations thereby hindering downstream interpretation
52 of cell state changes (Kester and Oudenaarden, 2018; Weinreb *et al.*, 2018). Although alternative non-
53 visual methods such as identifying dynamic driver-genes have been developed to help interpret
54 information from RNA velocity analysis (Bergen *et al.*, 2020), visual representation of cellular trajectories
55 remains an important approach to understanding the overall relationships between cell states.

56

57 Here, we developed VeloViz to visualize cellular trajectories by incorporating information about each
58 cell's predicted future transcriptional state inferred from RNA velocity analysis. Using both real and
59 simulated data representing cellular trajectories, we demonstrate that VeloViz embeddings are better able
60 to consistently capture underlying cellular trajectories across diverse trajectory topologies compared to
61 other evaluated methods. Likewise, given simulated cellular trajectories with missing intermediate cell
62 states, we find that VeloViz embeddings are able to more robustly retain the overall cell state relationships
63 in the underlying trajectories compared to other evaluated methods.

64

65

66 **2 Method**

67

68 In order to create an RNA-velocity-informed embedding, VeloViz uses each cell's current observed and
69 predicted future transcriptional states inferred from RNA velocity analysis to represent cells in the
70 population as a graph (Figure 1, Supplementary Information 1). Briefly, starting with spliced and
71 unspliced RNA counts from single-cell RNA-sequencing (scRNA-seq) data or cytoplasmic and nuclear
72 RNA counts from single cell molecular imaging data, the predicted future transcriptional state of cells are
73 inferred using RNA velocity pipelines such as velocity (La Manno *et al.*, 2018) or scVelo (Bergen *et al.*,
74 2020). We then optionally restrict to overdispersed genes (Fan *et al.*, 2016) and unit scale each gene's
75 variance, as well as mean center each gene's expression for the observed current and predicted future
76 transcriptional states, followed by dimensionality reduction by projecting these observed current and
77 predicted future transcriptional states into a common PC space. Using this reduced dimensional
78 representation of the observed current and predicted future transcriptional states, VeloViz then computes
79 a composite distance ($D_{A \rightarrow B} = -\cos(\theta_{AB}) * \frac{1}{\omega * d_{AB} + 1}$) between all cell pairs in the population. The
80 composite distance between two cells, Cell A and Cell B, takes into account: (1) their transcriptional
81 dissimilarity, defined as the Euclidean distance in the common PC space between Cell A's predicted future
82 state and Cell B's observed current state (d_{AB}) and (2) their velocity similarity, defined as the cosine
83 correlation between Cell A's velocity vector and the change vector representing the transition from Cell
84 A to Cell B (θ_{AB}). An additional tuning parameter (ω) weighs the relative importance of the transcriptional
85 similarity and the velocity similarity components. In this manner, the composite distance will be
86 minimized when Cell A's predicted future transcriptional state is similar to Cell B's observed current
87 transcriptional state and when the direction of Cell A's RNA velocity is similar to the direction of the
88 transition from Cell A to Cell B. Based on these composite distances, VeloViz creates a k-nearest neighbor

89 graph by assigning k directed, weighted edges from each cell to the k neighboring cells with smallest
90 composite distances. Edges are further pruned based on parameters that specify the minimum
91 transcriptional and velocity similarity in order to remove spurious cell state relationships. Finally, the
92 pruned graph can be visualized in 2D or 3D using graph layout or graph-embedding approaches such as
93 force-directed layout algorithms (Fruchterman and Reingold, 1991) or UMAP (McInnes *et al.*, 2018).

94

95

96 **3 Results**

97

98 3.1 Comparing VeloViz to other embeddings

99

100 To evaluate the performance of VeloViz, we first assessed VeloViz's ability to capture cellular
101 trajectories in simulated data representing cycling or branching trajectories (Supplementary Information
102 2). We compared the VeloViz embeddings to more conventional PC, t-SNE, UMAP, and diffusion map
103 embeddings. To evaluate how accurately each embedding captured the ground truth trajectory, we
104 calculated a trajectory consistency (TC) score (Supplementary Information 3, (Boggust *et al.*, 2019))
105 where high TC scores indicate more accurate representations of the ground truth trajectory. For the
106 simulated cycling trajectory, all evaluated embeddings were able to capture the cycling structure of the
107 trajectory except for the PC embedding (Supplementary Figure 1A). The TC score for the VeloViz
108 embedding was further higher than that of the PC, t-SNE, and UMAP embeddings. For the simulated
109 branching trajectory, the TC score for the VeloViz embedding was higher than TC scores for the t-SNE,
110 UMAP, and diffusion map embeddings (Supplementary Figure 1B-C). Likewise, we evaluated
111 VeloViz's ability to capture simultaneously cellular trajectories in conjunction with terminally
112 differentiated cell-types using simulated data representing both cycling or branching trajectories with
113 stable a cell population. For the simulated cycling trajectory with a stable cell population, all evaluated

114 embeddings were able to correctly distinguish the cycling and stable populations except for the PC
115 embedding (Supplementary Figure 1 D). Likewise, the VeloViz, t-SNE, UMAP, and diffusion map
116 embeddings preserved the cycling trajectory, while the PC embedding did not. The TC score for the
117 VeloViz embedding was higher than that of the other embeddings. For the simulated branching
118 trajectories with a stable cell population, all embeddings were able to separate the dynamic and stable
119 populations, but only the VeloViz and PC embeddings were able to capture the underlying branching
120 trajectory of the dynamic population (Supplementary Figure 1E-F). This is again reflected in the TC
121 scores, which are consistently higher for the VeloViz and PC embeddings compared to the TC scores for
122 the t-SNE, UMAP, and diffusion map embeddings. These simulation results demonstrate that VeloViz is
123 able to capture trajectories of various topologies compared to other embeddings, which may be better
124 suited for specific topologies.

125

126 Next, we assessed VeloViz's ability to capture cellular trajectories in scRNA-seq data. We applied
127 VeloViz to scRNA-seq data of mouse spermatogenic cells (Supplementary Information 4), where we
128 expect a developmental progression from spermatogonial stem cells to more differentiated spermatids
129 (Hermann *et al.*, 2018). For this simple, linear cellular trajectory, VeloViz was able to capture the overall
130 expected trajectory from secondary spermatocytes to early, mid, then late round spermatids
131 (Supplementary Figure 2). Generally, PCA, t-SNE, UMAP, and diffusion map were also able to capture
132 this expected trajectory. To assess VeloViz's ability to capture more complex trajectory structures, we
133 applied VeloViz to scRNA-seq data of the developing mouse pancreas (Supplementary Information 5),
134 where we expect to see both cycling and branching topologies at different stages of the trajectory. Briefly,
135 we expect cycling ductal cells to give rise to endocrine progenitor-precursor (EP) cells, which become
136 pre-endocrine cells that then differentiate into four hormone producing endocrine cell-types (Alpha, Beta,
137 Delta, and Epsilon cells) (Bastidas-Ponce *et al.*, 2019). We observed that while all evaluated embeddings
138 captured the progression of EP cells towards pre-endocrine cells, VeloViz, UMAP, and t-SNE embeddings

139 also captured the terminal branching differentiation into the different endocrine cell-types, which is not
140 clear in the PC or diffusion map embeddings (Figure 2). In addition, VeloViz was better able to capture
141 the cycling structure of ductal cells. Overall, these results indicate that VeloViz embeddings are able to
142 recapitulate expected trends from real scRNA-seq data

143

144 To explore the potential of using VeloViz with velocity estimated from other data types, we further applied
145 VeloViz to multiplexed error-robust fluorescent in situ hybridization (MERFISH) data (Xia *et al.*, 2019)
146 of cycling cultured U-2 OS cells (Supplementary Information 6). Again, we compared the VeloViz
147 embedding to embeddings constructed using PCA, t-SNE, and UMAP and found that all evaluated
148 embeddings, including VeloViz, were able to capture the expected cycling trajectory (Supplementary
149 Figure 3). In this manner, we find that VeloViz is able to capture cellular trajectories of diverse topologies
150 using both simulated and real data from multiple single cell transcriptomics technologies

151

152 3.2 Performance with missing intermediate cell states

153

154 While uniform sampling of the continuum of transcriptional states for cells along dynamic processes can
155 be used to infer how cell states may change over time, when sampling trajectories with rare or short-lived
156 intermediate cell states or when different cell states are differentially impacted by cell isolation protocols,
157 intermediate cell states may be lost leading to gaps in the observed cellular trajectory (Krishnaswami *et al.*
158 *al.*, 2016; Villani *et al.*, 2017; MacLean *et al.*, 2018; Moffitt *et al.*, 2018; Slyper *et al.*, 2020; Fan *et al.*,
159 2020). We hypothesized that incorporating information about each cell's predicted future transcriptional
160 state could enable VeloViz to more robustly construct representative cellular trajectories even when the
161 sampled cell states contain missing intermediate cell states or gaps in the underlying trajectory.

162

163 To evaluate the robustness of VeloViz in visualizing trajectories with such missing intermediate cell states,
164 we used simulated and real single cell transcriptomics data where some intermediate cells were removed,
165 creating a trajectory gap. Because t-SNE and UMAP preferentially preserve local cell-cell relationships,
166 we hypothesized that these embeddings would result in two distinct clusters of cells before and after the
167 simulated gap (Kobak and Berens, 2019; Heiser and Lau, 2020). Therefore, in addition to TC scores, we
168 calculated a gap distance (Supplementary Information 3), which measures the distance in the 2D
169 embedding space between cells before and after the simulated gap in the trajectory. Embeddings that
170 preserve the underlying trajectory despite this simulated gap will have a smaller gap distance. A small gap
171 distance between cells that are part of the same trajectory will facilitate a clearer depiction of the
172 underlying cell transitions compared to a large gap distance which may erroneously suggest that the cells
173 are unrelated.

174

175 Indeed, for the simulated cycling trajectory where cells corresponding to a segment of the cycle were
176 removed (Supplementary Information 2), VeloViz was the only embedding able to clearly represent the
177 cycling structure of the trajectory (Supplementary Figure 4A). The gap distance in the VeloViz embedding
178 was also smaller than in t-SNE, UMAP, and diffusion map embeddings. Likewise, for the simulated
179 branching trajectories where cells corresponding to a segment of an intermediate branch were removed
180 (Supplementary Information 2), only VeloViz and PCA were able to preserve the underlying topology
181 (Supplementary Figure 4B-C). The gap distance in the VeloViz embedding was smaller than that in the t-
182 SNE, UMAP, and diffusion map embeddings. In contrast, t-SNE and UMAP split cells before and after
183 the simulated gap into distinct clusters as expected. TC scores were also consistently higher for VeloViz
184 than with t-SNE, UMAP, and diffusion map embeddings. Similar trends were observed with simulated
185 data that included both dynamic cycling and branching populations with missing intermediate cell states
186 along with a stable cell population (Supplementary Figure 4D-F).

187

188 Likewise, for the U-2 OS MERFISH data, to simulate missing intermediate cell states, we removed cells
189 in the G2/M cell cycle phase. Briefly, we identified cells in the G2/M cell cycle phase by computing for
190 each cell a G2/M score based on the aggregated expression of canonical G2/M phase genes
191 (Supplementary Information 6). As before, we compared the VeloViz embedding to those constructed
192 with PCA, t-SNE, and UMAP. We found that VeloViz was better able to retain the cycling trajectory
193 despite the missing G2/M cells compared to the other evaluated embeddings (Supplementary Figure 5).

194

195 Similarly, for the developing mouse pancreas scRNA-seq data, to simulate missing intermediate cell
196 states, we removed pre-endocrine cells and used cell latent time (Bergen et al., 2020) to identify cells
197 before and after pre-endocrine cells in the developmental trajectory and to calculate gap distances in the
198 recalculated embeddings (Supplementary Information 5). Notably, while all embeddings depicted the
199 transition from ductal cells to endocrine progenitors, the subsequent transition from endocrine progenitors
200 into terminal endocrine cell-types was best captured by VeloViz. As expected, t-SNE and UMAP split
201 ductal and endocrine progenitor cells from terminal endocrine cell-types, which is reflected in the gap
202 distances (Figure 3). In particular, the position of endocrine progenitors and terminal endocrine cells and
203 the resulting velocity streams may lead to the interpretation that these two cell populations are
204 differentiating in two separate trajectories.

205

206 Still, because low dimensional representations can vary depending on parameter choices, we explored
207 the effect of changing these parameters on t-SNE and UMAP visualizations to see if certain parameter
208 choices would yield visualizations more representative of the underlying cellular trajectory. For t-SNE
209 embeddings, the perplexity parameter affects the extent to which the embedding reflects global vs. local
210 structure, with higher values resulting in embeddings that better preserve global structure (Kobak and
211 Berens, 2019). However, with a gap in the trajectory, the t-SNE embeddings result in two distinct
212 clusters of cells before and after the trajectory gap, even at large perplexity values (Supplementary

213 Figure 3). Likewise, for UMAP, we varied the values of two parameters: minimum distance, which
214 controls how densely packed points are in the embedding with small values resulting in more dense
215 clusters, and the number of neighbors, which functions similarly to perplexity in t-SNE (McInnes *et al.*,
216 2018). As with t-SNE, when embedding data with a simulated gap, UMAP is unable to capture the
217 expected trajectory even at large values of number of neighbors (Supplementary Figure 7). This
218 indicates that when intermediate cell states are missing, t-SNE and UMAP embeddings may be unable to
219 recapitulate the expected underlying trajectory structure regardless of parameter choices. Overall, we
220 find that VeloViz is able to visualize a more reliable representation of underlying trajectories even when
221 intermediate cell states may be missing.

222

223 3.3 Scalability

224 Given the increasing availability of large single cell transcriptomics datasets (Lähnemann *et al.*, 2020),
225 we sought to evaluate the scalability of VeloViz with increasing cell numbers. Briefly, we down-sampled
226 a dataset of approximately 10,000 cells (10X Genomics, 2020) to create datasets ranging from 100 cells
227 to 9295 cells. For each dataset, we calculated velocity using *velocyto.R* and constructed an embedding
228 using VeloViz while evaluating runtime and memory usage (Supplementary Information 7). We find that
229 both runtime and memory usage of VeloViz scales linearly with the number of cells and is comparable to
230 that of RNA velocity estimations (Supplementary Figure 8).

231

232

233 4 Discussion

234 In order to facilitate better visual representation of relationships between cell states in single cell
235 transcriptomic data, we developed VeloViz to create low dimensional embeddings that incorporate
236 dynamic information inferred from RNA velocity. We find that VeloViz is able to visualize cellular
237 trajectories of diverse topologies and capture global cell state relationships, even when intermediate cell

238 states may be missing. Particularly when intermediate cell states are missing, we find that visualization
239 with t-SNE and UMAP may result in distinct clusters containing cells before and after trajectory gaps,
240 leading to erroneous interpretation that cells are part of biologically distinct subpopulations rather than
241 the same biological trajectory.

242

243 However, several limitations of VeloViz should be considered when using VeloViz embeddings to
244 interpret putative cellular trajectories. Embeddings constructed using VeloViz incorporate multiple user
245 inputted hyperparameters (Supplementary Information 1). We explored the effects of changing these
246 parameters on the visualization of simulated cycling trajectories with missing intermediates and the
247 resulting TC scores (Supplementary Figure 9). We found that the VeloViz embedding was most robust
248 to changes in cosine similarity threshold (t_i) and most sensitive to changes in k . However, without *a*
249 *priori* knowledge of expected relationships between cell subpopulations, it may be challenging to find
250 the optimal parameter set that yields the most representative embedding. Furthermore, different
251 components of the trajectory being visualized, such as gaps versus branching structures, may have
252 different optimal parameters. Thus, a range of hyperparameters may need to be explored to evaluate the
253 stability of visualized cellular trajectories. Further limitations of VeloViz extend from the limitations of
254 RNA velocity analysis in general. Notably, RNA velocity analysis can only infer cell state changes that
255 are determined by changes in gene expression. Other molecular features such as alternative splicing,
256 chromatin state, post-translational modifications, differential localization, and cell microenvironment
257 that contribute to cell state changes are not considered in RNA velocity analysis, and therefore these cell
258 state changes will not be represented in the VeloViz embedding (Weinreb *et al.*, 2018; Tritschler *et al.*,
259 2019). In addition, it remains unknown the degree to which cell state changes are stochastic i.e. the
260 probability that two cells with similar transcriptional states will develop differently. This stochasticity
261 may limit the accuracy of predicting future cell state based on current gene expression dynamics.

262 Ultimately, insights gained from RNA velocity analysis should be considered within the context of other

263 available data, such as differential gene expression, mutational analysis, and targeted experimental
264 validation.

265

266 Overall, by taking into account the predicted future transcriptional states of cells from RNA velocity
267 analysis, VeloViz provides an additional approach for visualizing putative cellular trajectories to aid in
268 the interpretation of cellular dynamics from single cell transcriptomics data.

269

270

271 **Funding:** This work was supported by the National Institutes of Health [T32GM136577 to L.A.]

272

273 **Conflict of Interest:** none declared.

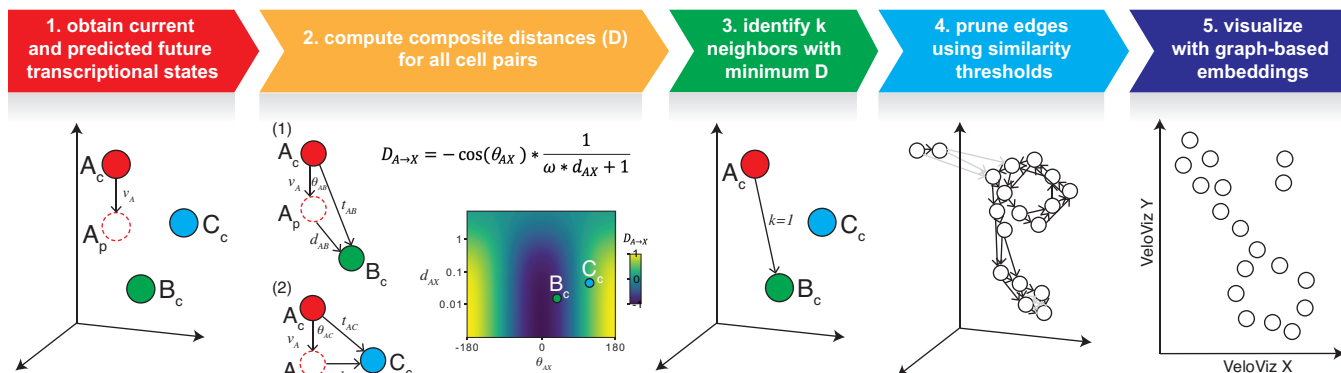
274

275 References

- 276 10X Genomics (2020) 10k Mouse E18 Combined Cortex, Hippocampus and Subventricular Zone Cells,
277 Single Indexed.
- 278 Bastidas-Ponce,A. *et al.* (2019) Comprehensive single cell mRNA profiling reveals a detailed roadmap
279 for pancreatic endocrinogenesis. *Development*, **146**.
- 280 Bergen,V. *et al.* (2020) Generalizing RNA velocity to transient cell states through dynamical modeling.
281 *Nat. Biotechnol.*, 1–7.
- 282 Boggust,A. *et al.* (2019) Embedding Comparator: Visualizing Differences in Global Structure and Local
283 Neighborhoods via Small Multiples. *ArXiv191204853 Cs*.
- 284 Coifman,R.R. *et al.* (2005) Geometric diffusions as a tool for harmonic analysis and structure definition
285 of data: Diffusion maps. *Proc. Natl. Acad. Sci.*, **102**, 7426–7431.
- 286 Fan,J. *et al.* (2016) Characterizing transcriptional heterogeneity through pathway and gene set
287 overdispersion analysis. *Nat. Methods*, **13**, 241–244.
- 288 Fan,J. *et al.* (2020) Single-cell transcriptomics in cancer: computational challenges and opportunities.
289 *Exp. Mol. Med.*, **52**, 1452–1465.
- 290 Fruchterman,T.M.J. and Reingold,E.M. (1991) Graph drawing by force-directed placement. *Softw.*
291 *Pract. Exp.*, **21**, 1129–1164.
- 292 Heiser,C.N. and Lau,K.S. (2020) A Quantitative Framework for Evaluating Single-Cell Data Structure
293 Preservation by Dimensionality Reduction Techniques. *Cell Rep.*, **31**, 107576.
- 294 Hermann,B.P. *et al.* (2018) The Mammalian Spermatogenesis Single-Cell Transcriptome, from
295 Spermatogonial Stem Cells to Spermatids. *Cell Rep.*, **25**, 1650-1667.e8.
- 296 Kester,L. and Oudenaarden,A. van (2018) Single-Cell Transcriptomics Meets Lineage Tracing. *Cell*
297 *Stem Cell*, **23**, 166–179.
- 298 Kobak,D. and Berens,P. (2019) The art of using t-SNE for single-cell transcriptomics. *Nat. Commun.*,
299 **10**, 5416.
- 300 Krishnaswami,S.R. *et al.* (2016) Using single nuclei for RNA-seq to capture the transcriptome of
301 postmortem neurons. *Nat. Protoc.*, **11**, 499–524.
- 302 La Manno,G. *et al.* (2018) RNA velocity of single cells. *Nature*, **560**, 494–498.
- 303 Lähnemann,D. *et al.* (2020) Eleven grand challenges in single-cell data science. *Genome Biol.*, **21**, 31.
- 304 Maaten,L. van der and Hinton,G. (2008) Visualizing Data using t-SNE. *J. Mach. Learn. Res.*, **9**, 2579–
305 2605.
- 306 MacLean,A.L. *et al.* (2018) Exploring intermediate cell states through the lens of single cells. *Curr.*
307 *Opin. Syst. Biol.*, **9**, 32–41.
- 308 McInnes,L. *et al.* (2018) UMAP: Uniform Manifold Approximation and Projection. *J. Open Source*
309 *Softw.*, **3**, 861.
- 310 Moffitt,J.R. *et al.* (2018) Molecular, spatial, and functional single-cell profiling of the hypothalamic
311 preoptic region. *Science*, **362**.
- 312 Saelens,W. *et al.* (2019) A comparison of single-cell trajectory inference methods. *Nat. Biotechnol.*, **37**,
313 547–554.
- 314 Slyper,M. *et al.* (2020) A single-cell and single-nucleus RNA-Seq toolbox for fresh and frozen human
315 tumors. *Nat. Med.*, **26**, 792–802.
- 316 Tritschler,S. *et al.* (2019) Concepts and limitations for learning developmental trajectories from single
317 cell genomics. *Development*, **146**.
- 318 Villani,A.-C. *et al.* (2017) Single-cell RNA-seq reveals new types of human blood dendritic cells,
319 monocytes, and progenitors. *Science*, **356**.
- 320 Weinreb,C. *et al.* (2018) Fundamental limits on dynamic inference from single-cell snapshots. *Proc.*
321 *Natl. Acad. Sci.*, **115**, E2467–E2476.

- 322 Xia,C. *et al.* (2019) Spatial transcriptome profiling by MERFISH reveals subcellular RNA
323 compartmentalization and cell cycle-dependent gene expression. *Proc. Natl. Acad. Sci.*, **116**,
324 19490–19499.
- 325 Zhang,Q. *et al.* (2019) Landscape and Dynamics of Single Immune Cells in Hepatocellular Carcinoma.
326 *Cell*, **179**, 829-845.e20.
- 327 Zywitza,V. *et al.* (2018) Single-Cell Transcriptomics Characterizes Cell Types in the Subventricular
328 Zone and Uncovers Molecular Defects Impairing Adult Neurogenesis. *Cell Rep.*, **25**, 2457-
329 2469.e8.
- 330
- 331
- 332

333 **Figures**



334

335

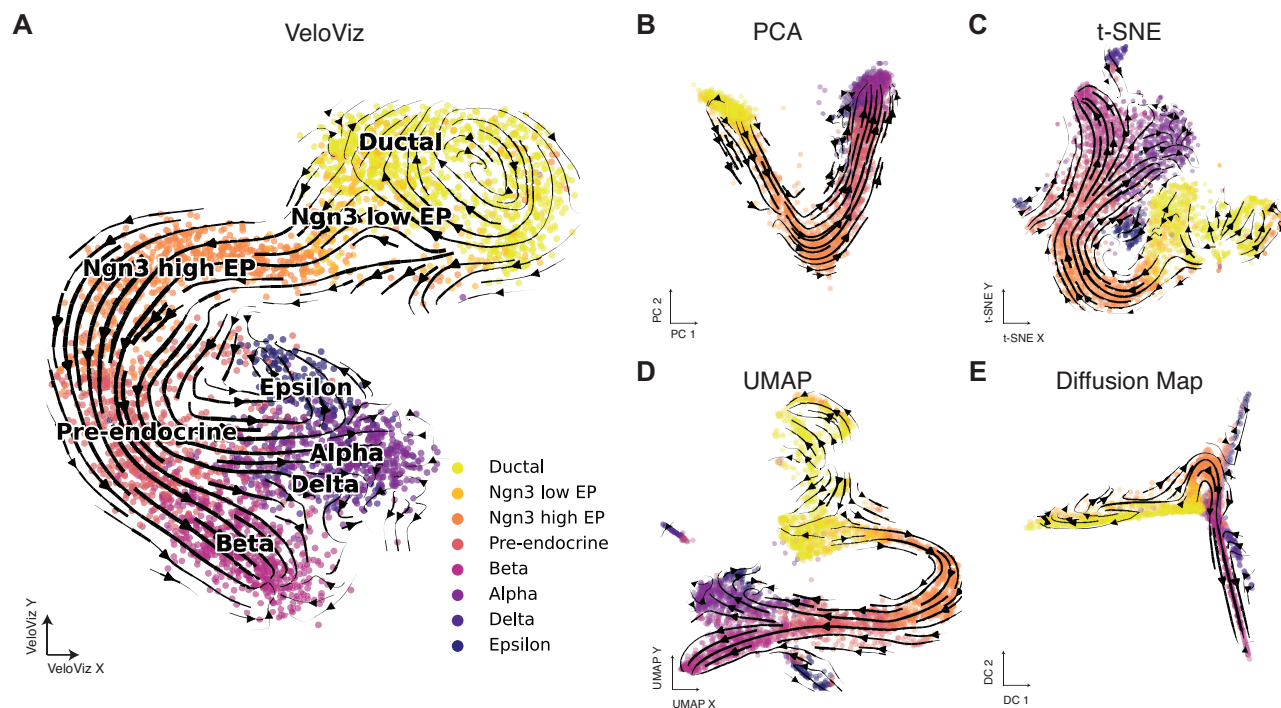
336 **Figure 1. Overview of VeloViz.** RNA-velocity informed embeddings are created by VeloViz in five
 337 steps: 1) The observed current (X_c) and predicted future (X_p) transcriptional cell states are inferred from
 338 RNA velocity and reduced into a common PC space; 2) composite distances (D) between all cell pairs are
 339 computed. The composite distance from Cell A to Cell X ($D_{A \rightarrow X}$) takes into account the similarity in
 340 transcriptional profiles (d_{AX}) between Cell X's observed current (X_c) and Cell A's predicted future
 341 transcriptional state (A_p), and the cosine correlation between Cell A's RNA-velocity (v_A) and the change
 342 vector (t_{AX}) representing a transition from Cell A's current state (A_c) to Cell X's current state (X_c). A
 343 distance weight (ω) is used to adjust the relative importance of transcriptional similarity and cosine
 344 correlation in the composite distance; 3) each cell is represented as a node in a graph, and for each cell,
 345 graph edges are assigned to the k cells with the minimum composite distances. Edge weights are computed
 346 based on composite distances as $weight_{AB} = \max(D) - D_{AB}$; 4) edges assigned in 3. are pruned (in grey)
 347 using transcriptional and velocity similarity thresholds. Edge shade corresponds to edge weight computed
 348 based on composite distance, with darker arrows representing edges with larger weights; 5) the resulting
 349 graph can be visualized as a 2D or 3D embedding using graph-based embedding approaches.

350

351

352

353



354

355

356

Figure 2. VeloViz reconstructs trajectories from pancreatic endocrinogenesis scRNA-seq. 2D

357

embeddings visualizing pancreatic endocrinogenesis generated using VeloViz (A), PCA (B), t-SNE (C),

358

UMAP (D), and diffusion mapping (E). Cells are colored by cell state annotations provided in (Bergen

359

et al., 2020). Arrows show the projection of velocities derived from dynamical velocity modelling

360

(Bergen *et al.*, 2020) onto the embeddings.

361

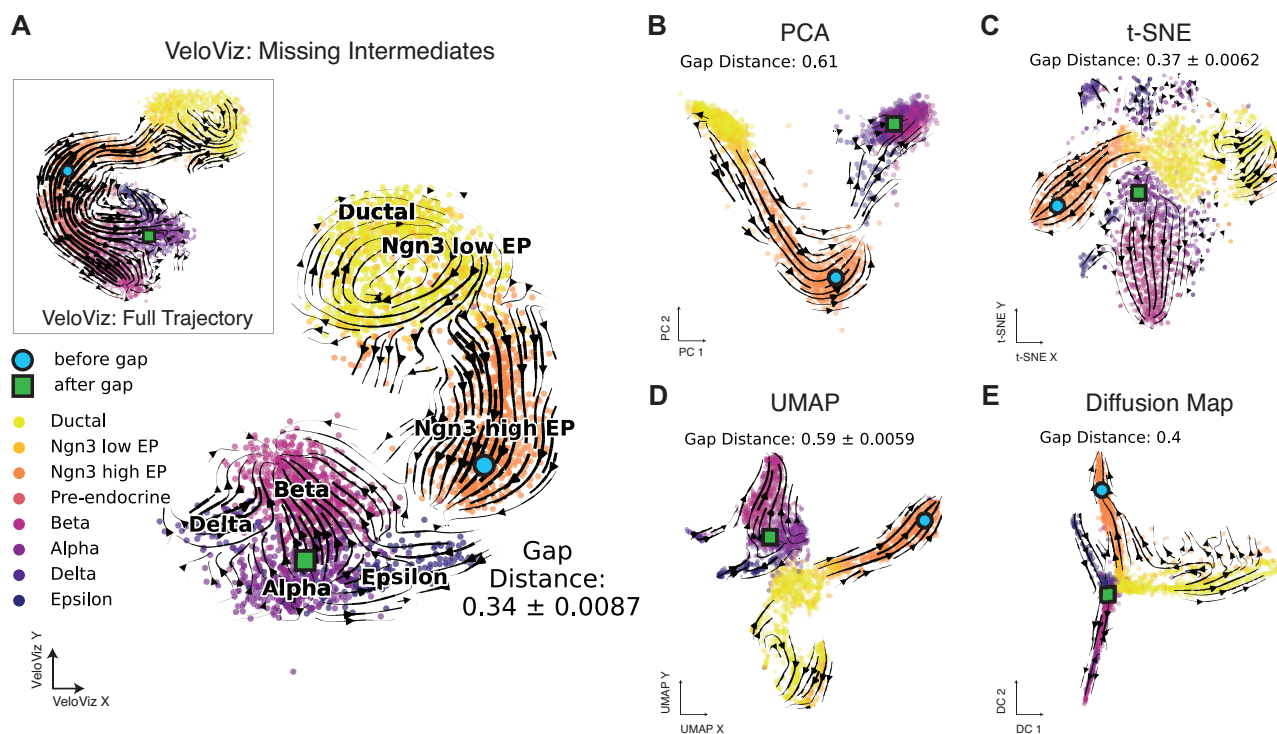
362

363

364

365

366



367

368 **Figure 3. VeloViz reconstructs trajectories from pancreatic endocrinogenesis scRNA-seq data with**
369 **missing intermediates. A)** VeloViz 2D embedding visualizing pancreatic endocrinogenesis with pre-
370 endocrine intermediates removed creating a gap in the developmental trajectory. Inset shows the VeloViz
371 embedding of the full dataset. Cells are colored by cell state annotations provided in (Bergen *et al.*, 2020).
372 Arrows show the projection of velocities derived from dynamical velocity modelling onto the VeloViz
373 embeddings. Gap distances measure the median distance in the 2D embedding between the 300 cells
374 before and after pre-endocrine cells in the developmental trajectory (Supplementary Information 3iii).
375 Blue circle and green square indicate the median coordinates of cells before and after pre-endocrine cells
376 in the developmental trajectory, respectively. **B-E)** 2D embeddings visualizing pancreatic
377 endocrinogenesis with removed pre-endocrine intermediates using PCA, t-SNE, UMAP, and diffusion
378 mapping, respectively with arrows showing the projection of velocities derived from dynamical velocity
379 modelling.